

# Molecular Dynamics Simulation of Sonoluminescence: Modeling, Algorithms and Simulation Results

Steven J. Ruuth\*, Seth Putterman<sup>†</sup> and Barry Merriman<sup>‡</sup>

Dec. 30, 2000

## Abstract

Sonoluminescence is the phenomena of light emission from a collapsing gas bubble in a liquid. Theoretical explanations of this extreme energy focusing are controversial and difficult to validate experimentally. We propose to use molecular dynamics simulations of the collapsing gas bubble to clarify the energy focusing mechanism, and provide insight into the mechanism of light emission.

In this paper, we model the interior of a collapsing noble gas bubble as a hard sphere gas driven by a spherical piston boundary moving according to the Rayleigh-Plesset equation. We also include a simple treatment of ionization effects in the gas at high temperatures. By using fast, tree-based algorithms, we can exactly follow the dynamics of million particle systems during the collapse. Our results clearly show strong energy focusing within the bubble, including the formation of shocks, strong ionization, and temperatures in the range of 50,000—500,000 degrees Kelvin. Our calculations show that the gas-liquid boundary interaction has a strong effect on the internal gas dynamics.

---

\*Department of Mathematics, Simon Fraser University. ([sruuth@sfu.ca](mailto:sruuth@sfu.ca)). The work of this author was partially supported by DARPA and NSERC Canada.

<sup>†</sup>Department of Physics, University of California at Los Angeles. The work of this author was partially supported by DARPA.

<sup>‡</sup>Department of Mathematics, University of California at Los Angeles. ([barry@math.ucla.edu](mailto:barry@math.ucla.edu)). The work of this author was partially supported by DARPA.

We also estimate the duration of the light pulse from our model, which predicts that it scales linearly with the ambient bubble radius.

As the number of particles in a physical sonoluminescing bubble is within the foreseeable capability of molecular dynamics simulations we also propose that fine scale sonoluminescence experiments can be viewed as excellent test problems for advancing the art of molecular dynamics.

## 1 Introduction

### 1.1 Background

As a gas bubble in a liquid collapses, the potential energy stored during its prior expansion is released and strongly focused. The extent of focusing can be so great that a burst of light is emitted at the final stage of collapse. This process can be driven repeatedly by exciting bubbles with a sound field, and the resulting transduction of sound into light is known as sonoluminescence (SL) [10, 30, 11, 2, 24, 1].

Sonoluminescence can be observed in dense fields of transient cavitation bubbles produced by applying intense sound to a liquid, or in a periodic single bubble mode which allows more detailed experimental observations. In single bubble SL, a single gas bubble in the liquid is created and periodically driven to expand and collapse by an applied sound field. The bubble begins its cycle of evolution as the low pressure phase of the sound field arrives, causing it to expand to a maximal radius. As the applied acoustic pressure increases, the bubble begins to collapse, first reaching its ambient radius and corresponding ambient pressure and internal temperature, and then radially collapsing further, with the bubble walls falling inward driven by the rising external fluid pressure. The collapse accelerates rapidly, until gas trapped inside the bubble is compressed and heated to a pressure that ultimately halts and reverses the motion of the bubble walls. Thus the bubble reaches a minimum radius, and then rapidly “bounces” back to a much larger size. At some point near the minimum radius, the resulting internal “hot spot” can release a burst of light. While the basic bubble collapse dynamics can be observed for a variety of gas and liquid combinations, light emission typically requires the bubble to contain sufficient noble gas, and works particularly well in water.

The mechanism of light emission from the gas is not understood, nor is much known about related quantities such as peak temperatures, pressures or levels of ionization.

## 1.2 Limitations of Hydrodynamic Models

It is known that the mechanical conditions during collapse of a common gas bubble in water are quite extreme: as the bubble reaches sub-micron diameter, the bubble wall experiences accelerations that exceed  $10^{11}g$  and supersonic changes in velocity that occur on picosecond time scales. In order to understand how this affects the state of the internal gas, the standard approach is to apply continuum fluid mechanics. Some models assume that pressure and temperature are uniform inside of the collapsed bubble [16] while other theories calculate the effects of imploding shock waves [1, 35, 14, 22]. Various fluid models have been applied both at non-dissipative (Euler Equations) and dissipative (Navier-Stokes Equations) levels of description [19, 31, 36, 23].

All these fluid approaches are limited in their predictive power by the need to represent transport processes and the equation of state. Under such extreme flow conditions, little is known about these effects and one is forced to extrapolate from known forms. The net result is that the modeling predictions directly reflect these assumptions. This is not satisfactory for the purpose of understanding what actually occurs within the bubble.

An especially fundamental limitation of continuum mechanical approaches is the assumption of local thermodynamic equilibrium, i.e. it is assumed that the macroscopic fluid variables do not change much over molecular length and time scales. Although the bubble starts out in such a state, its subsequent runaway collapse ultimately leads to a regime where this clearly does not hold. In this state, from which the ultraviolet picosecond flash of light is emitted, one can question the basic applicability of hydrodynamic models.

## 1.3 Molecular Dynamics Modeling

We propose to remove the assumption of thermodynamic equilibrium, and also eliminate any controversy over the correct equation of state, by using molecular dynamics (MD) simulations of the gas dynamics within the bubble. In this approach, we directly apply Newton's laws of motion to the

gas molecules, including as much detail as is desired (or practical) about the molecular collisions and related atomic physics. While this approach is computationally intensive, it delivers to us a clear, physical picture of what actually transpires during the bubble collapse. With the inclusion of sufficient detail and efficient programming, it could ultimately allow the simulation of the light emission process itself.

While the small length and time scales of sonoluminescence present major obstacles for hydrodynamic modeling, they actually make it ideal for molecular dynamics: precisely because the final system is so small, it becomes possible to do a complete MD simulation of the collapse. In fact, sonoluminescence is somewhat unique in this regard. Usually the systems directly simulated with molecular dynamics are many orders of magnitude smaller—fewer particles, shorter time scales—than the corresponding systems realized in experiments or in nature, and this gap is too large to be eliminated by increases in computing power [28]. In contrast, the number of particles within the interior of a small SL bubble is comparable to the number of simulation particles that can be handled with current computational facilities.

For example, a typical SL bubble driven at 30kHz has an ambient radius of  $6 \mu m$  and contains  $2.25 \times 10^{10}$  particles. At the extreme, SL bubbles containing on the order of several million particles have been observed in systems driven at Megahertz frequencies [32]. This compares well with simulations, where we have been able to compute the gas dynamics of a one million particle bubble collapse using a run time of a few days on a single processor workstation-grade computer. Parallel processing simulations would make 10 to 100 million particle simulations feasible. As the number of simulation particles reaches that in real systems, the remaining computer power can be used to add in more complex atomic physics, and thus allow more detailed study of the processes involved.

## 1.4 Predictive Modeling Goals

The overall goal of the MD modeling is to generate a better understanding of the processes that result in energy focusing and light emission during SL. This is to be accomplished through a dual approach of model prediction and model validation: we use the model to illustrate the phenomena that cannot be experimentally observed during the collapse, and also to make predictions that can be experimentally validated.

The basic experimental unknown in SL is the degree of energy focusing that is achieved inside of the bubble. For example, the spectral density of light from helium bubbles in water is still increasing at wavelengths as short as 200nm (energy exceeding 6 eV) where the extinction coefficient of water cuts off the measurement [1]. Related to the question of energy focusing are the detailed questions of whether there is shock formation within the bubble, whether there is plasma formation, and what peak temperatures are achieved during the collapse. For example, the most extreme theoretical estimates suggest that the interior may reach temperatures sufficient to induce deuterium-tritium fusion [3]. Over the range of parameter space studied, shock formation and strong ionization appear to be typical, and the *lowest* peak temperatures found in our simulations are about 40,000K, with the highest approaching 500,000K. Our findings also indicate that boundary conditions strongly affect the interior motion. With a low, fixed temperature (i.e. heat bath) condition the peak temperatures and internal gradients are higher than for adiabatic motion.

A key experimental observable in SL is the duration of the light flash, or “flash width” [2], because knowledge of this puts constraints on the underlying mechanism of light emission. This can be used as a validation point for any model or theory. For example, volume radiation from a plasma will yield a different flash width than surface radiation from a black body. Since our simulations do not include fundamental radiative mechanisms such as atomic excitation or charged particle acceleration, our current MD model cannot directly determine the light emitting mechanism or the flash width. However, a prediction about the flash width can be obtained from our calculation of the peak temperature as a function of time, assuming the light emission occurs while the peak temperature is high. Our simulations for Helium show that simple adiabatic compression does not produce a sharp temperature spike in time, but the thermal boundary condition causes a spike with a duration that scales with the ambient bubble radius. This result predicts that the flash width should scale with the ambient bubble radius. If valid, this scaling suggests that at high acoustic frequencies [ $\sim 10\text{MHz}$ ] [32] the duration of a SL flash could be about equal to or less than 1 ps.

## 1.5 Outline of the Paper

The outline of the paper follows: Section 2 describes the model for the bubble collapse in detail. Section 3 outlines the principle algorithms used to evolve the hard sphere system. Section 4 provides detailed results from our MD simulations. Finally, Section 5 concludes a summary of our observations, and lists interesting future areas of investigation suggested by this first attempt at molecular dynamics modeling of sonoluminescence.

## 2 Modeling Sonoluminescence Bubbles

In this section, we present our Molecular Dynamics model for SL bubbles. The overall strategy is to model the system as a spherical piston that compresses a gas of hard spheres, with energy deducted from the system for ionization events at higher temperatures. The details and motivations for this are given in the following subsections.

### 2.1 Model Parameters

We want to focus on the simulation of single bubble sonoluminescence, so that results can be compared to the best studied experimental SL systems. Such bubbles remain spherical during their collapse [33], and their behavior is parameterized by their ambient radius (the radius they have when at rest at the ambient pressure) and their maximum radius (the radius they attain when maximally expanded at the low pressure point of the applied sound field).

We cannot directly simulate all such SL bubbles, since they may contain several orders of magnitude more gas particles than our computational budget can accommodate. Typically, we can afford to do a calculation with some given number of simulation particles,  $N$ , and the question becomes how large of a bubble can we directly simulate. The ambient radius,  $R_0$ , is related to the number of gas particles,  $N$ , by the ideal gas equation of state

$$P_0 \left( \frac{4}{3} \pi R_0^3 \right) = kT_0 N$$

where  $T_0 = 300K$  and  $P_0 = 1 \text{ atm}$  are the ambient temperature and pressure, and  $k$  is Boltzmann's constant. Thus we see that the fewer the simulation

particles we use, the smaller the ambient size of the bubble being simulated.

Once the ambient size is determined by our simulation budget, we are however free to choose any maximum radius. For experimentally relevant simulations, the maximum radius  $R_m$  is chosen to yield the same ratio of  $R_m/R_0$  [ $\sim 10$ ] for the MD simulation as is seen in experimental SL bubbles. This is natural because this ratio is a measure of the available energy stored in the expansion, since the stored energy/particle due to the work done by expanding to the maximum volume  $V_m$  against the applied pressure  $P_0$  is

$$\frac{P_0 V_m}{N} = kT_0 \frac{R_m^3}{R_0^3}.$$

## 2.2 Bubble Collapse

Since the bubble remains spherical during collapse, its boundary dynamics are described entirely by the radius as a function of time,  $R(t)$ . We are concerned with energy focusing processes and gas dynamics inside the bubble, and in this spirit we will take  $R(t)$  as being known. A convenient model of the spherical piston that captures some qualitative features of the supersonic collapse is provided by Rayleigh's equation [24]

$$R\ddot{R} + \frac{3}{2}\dot{R}^2 = [P_g(R) - P_0]/\rho, \quad (1)$$

with a van der Waals hard core equation of state

$$P_g(R) = \frac{P_0 R_0^{3\gamma}}{(R^3 - a^3)^\gamma}, \quad (2)$$

$\gamma = 5/3$ , where  $a$  is the radius of the gas in the bubble when compressed to its van der Waals hard core ( $R_0/a = 10.1, 9.15, 7.84$  for He, Ar, Xe),  $\rho$  is the density of the surrounding fluid, and the initial condition for the solution to (1) is that  $\dot{R} = 0$  when  $R = R_m$ . We emphasize that the derivation of Equations (1,2) applies only for small Mach number motion and thus they are invalid as a fundamental theory for SL [9]. However, in this first attempt to simulate SL with molecular dynamics we are interested in possible focusing processes within the bubble and use of (1,2) as a launch condition appears appropriate since the resulting  $R(t)$  reasonably approximates the gross bubble pulsation [24].

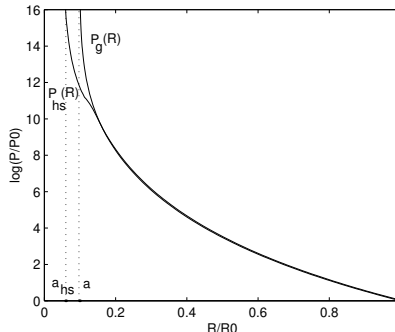


Figure 1: Plots of the adiabatic equations of state for the van der Waals pressure  $P_g(R)$  and the computed hard sphere pressure  $P_{hs}(R)$  for Helium.

Consistent with this approximation, viscous damping and acoustic radiation have also been neglected. At the next level of simulation one should include a self-consistently determined boundary condition on pressure at the bubble's wall. In this way, energy loss due to acoustic radiation is properly accounted for.

As a point of comparison, it is worth noting that the adiabatic equations of state for the van der Waals pressure  $P_g(R)$  and the computed *equilibrium* hard sphere pressure  $P_{hs}(R)$  (the equilibrium pressure as a function of radius as the radius is decreased *slowly* on the hard spheres) agree very well, except at bubble radii near the hard core, as graphed in Figure 1 for Helium (with the other noble gases also in good agreement, except near the hard core). At small radii, the van der Waals pressure diverges as  $R$  tends to  $a$  and the  $P_{hs}(R)$  diverges as  $R$  tends to

$$a_{hs} \equiv \left( \frac{N}{0.63} \right)^{1/3} \frac{\sigma}{2}$$

which is the minimum radius for random closed packing [29].

### 2.3 Gas Dynamics

It has been observed that for SL in water, the bubble must contain sufficient amounts of a noble gas. Thus in many single bubble SL experiments, the water is first de-gassed to remove atmospheric gases, and then re-saturated



with a noble gas to produce pure noble gas bubbles. We will focus our gas dynamic model on this system, since it is a frequent experimental model and also because it allows the simplest molecular gas dynamics models. Because the gas is noble, it consists of isolated atoms that do not engage in chemical reactions. Thus we can model it with simple gas particles that have no rotational or internal vibrational degrees of freedom, and which do not engage in any chemical reactions with the water walls of the bubble, even at elevated temperatures.

Molecular dynamics simulations for such simple gas particles fall into two broad categories, defined by the way they treat interatomic forces. The forces can either be given by a potential that varies continuously with radius from the atom center (“soft sphere”), or by a potential that is a step function of radius (“hard sphere”). The latter particles behave simply like billiard balls. While the continuous potential are more physically realistic, they are also much more costly to compute with. This is because numerical time integration methods must be used to compute the particle motions in response to the continuously varying forces, and the time step must be small enough to accurately resolve all particle trajectories in the system. Thus the motion of a few fast moving particles will force the use a small, costly timestep for all particles in the system. In contrast, step potentials do not experience this problem because they evolve in time by a series of discrete collision events. No explicit numerical integration is needed since impulsive collisions are carried out only when atoms interact, and between collisions each atom follows an independent linear trajectory. Thus each atom effectively uses its own optimally large timestep, instead of an excessively small step imposed by the the fastest particles in the system. Moreover, there is no numerical integration error because trajectories are evaluated to within the roundoff error of the machine. [28]

Because of this difference in computational cost, it is desirable to use the hard sphere model if it can capture the physics of interest. In our case, we want to get accurate gas dynamics at mid to high energies for fairly large numbers of particles. Whether hard spheres are sufficient to model this regime in an SL bubble is an empirical question, but such models have been shown to yield accurate predictions of noble gas viscosity from room temperature up to the gas ionization temperatures [5]. We take this to be a reasonable validation that a hard sphere gas provides a good model for the gas dynamics encountered during bubble collapse, at least up to ionization

temperatures. Near that point and beyond, it also seems reasonable that a hard sphere model applies, since the softer parts of the potential are all the more insignificant for high energy collisions.

The dynamics of a hard sphere system involve processing impulsive collisions at the collision times. To illustrate, consider two particles separated by a relative position  $\mathbf{r}$  and having a relative velocity  $\mathbf{v}$ . These particles collide if their separation equals the atomic diameter  $\sigma$  at some time  $\tau$  in the future. If such a collision occurs, then  $\tau$  is the smaller positive solution of

$$|\mathbf{r} + \mathbf{v}\tau| = \sigma$$

which has a solution

$$\tau = -\frac{1}{\mathbf{v} \cdot \mathbf{v}} \left( \mathbf{r} \cdot \mathbf{v} + \sqrt{(\mathbf{r} \cdot \mathbf{v})^2 - \mathbf{v} \cdot \mathbf{v}(\mathbf{r} \cdot \mathbf{r} - \sigma^2)} \right)$$

Collisions are carried out impulsively so that the change in velocities preserves energy and momentum. Specifically,

$$\Delta \mathbf{v}_1 = -\Delta \mathbf{v}_2 = -\frac{(\mathbf{r}_c \cdot \mathbf{v})\mathbf{r}_c}{\sigma^2}$$

where  $\Delta \mathbf{v}_1$  is the change in velocity of the first particle,  $\Delta \mathbf{v}_2$  is the change in velocity of the second particle and  $\mathbf{r}_c$  is the relative position at the time of collision.

Extensions to step potentials that consist of a hard repulsive core surrounded by an attractive well are also possible. See [28] for details.

## 2.4 Bubble Wall Boundary Conditions

When a gas particle hits the bubble wall, it might simply be directed back into the interior by a strong collision with a liquid molecule, or it may penetrate into the liquid, undergoing multiple thermalizing collisions. In the latter case, assuming the liquid is already saturated with gas atoms, the thermalized atom (or an equivalent one from the saturated liquid reservoir) will ultimately random walk its way back into the bubble interior.

For our MD model, we will idealize these two modes of boundary interaction as either as energy conserving *specular* collisions or as a *heat bath* boundary conditions.

For the case of specular collisions, particles reflect from the boundary with a speed equal to the collision speed in the local rest frame of the wall. The direction of propagation is determined according to the law of reflection, where the angle of incidence equals the angle of reflection with respect to the local normal to the bubble surface.

For heat bath boundary conditions, when a particle hits the boundary it is assigned a thermal velocity at the ambient liquid temperature  $T_0$ , and the direction of propagation back into the interior is chosen according to a suitable angular distribution. We ignore the small time lag that might exist between exit and reentry for the thermalized gas particle.

For the angular distribution, we use the *cosine distribution*, where the angle of reflection  $\theta$  is assigned randomly according to a probability density function,

$$f(\theta) = \begin{cases} (1/2) \cos \theta & \text{for } -\pi/2 \leq \theta \leq \pi/2 \\ 0 & \text{otherwise} \end{cases}$$

We have also tried a uniform distribution in angle in selected test cases. This did not significantly change the simulation results. (Nonetheless, we note that there may exist situations where results differ qualitatively since a uniform distribution has a greater tendency to cause reflected particles to build up near the wall.)

In reality, we expect that the physical boundary will have some characteristics of both models. By investigating these extreme cases we hope to see the full range of effects that boundary conditions can have on the bubble dynamics.

## 2.5 Initialization

Initially the bubble is its maximum radius, ( $R = R_m$ ), and particles are moving in uniformly distributed random directions, with the same thermal speed  $v_{th}(T_i) = \sqrt{3T_i k/m}$ , where  $T_i$  is the initial temperature and  $m$  is the mass of the particle. Randomization of speeds is not necessary, since the particles rapidly thermalize their energies in any case. For heat bath boundary conditions, the initial temperature is taken to be the ambient temperature,  $T_i = T_0$ , reflecting the thermalization with the liquid. With specular boundary conditions this choice generates unphysically large temperatures when the bubble collapses to its ambient size, due to adiabatic heating. In or-

der to achieve the ambient temperature  $T_0$  at the ambient radius  $R_0$ , the initial temperature must be scaled down to  $T_i = T_0/(R_m/R_0)^2 = T_0/100$ . The factor of  $(R_0/R_m)^2$  approximately cancels the adiabatic heating (since  $TR^2 = \text{constant}$  in a  $\gamma = 5/3$  ideal gas at constant entropy) during the initial, slow portion of the collapse.

## 2.6 Hard Sphere Properties

The basic properties associated with the hard sphere model are the gas particle mass and diameter. The mass is simply taken to be the mass of the noble gas atom being simulated. See Table I below. The choice of proper hard sphere diameter is a much more difficult question. The diameter should represent the statistical average distance of approach of the particles during collisions, and thus in general it should depend on the collision energy.

In our most basic model we will neglect this temperature dependence and choose particle diameters that have been derived from the kinetic theory for the viscosity of a gas at room temperature [17, 26, 25]:

Gas	Mass [g/mole]	Diameter [Å]
He	4.00	2.18
Ar	39.95	3.66
Xe	131.29	4.92

Table I. Hard Sphere Diameters and Masses

To produce a more realistic model for higher temperature regimes of interest in SL, the hard sphere diameter should depend on the relative velocity of the colliding particles. A variety of models have been proposed to take this effect into account [5]. These include the variable hard sphere (VHS) model [4], the variable soft sphere (VSS) model [20, 21] and the generalized hard sphere (GHS) model [15] which is an extension of the VHS and VSS models. In this report, we are mainly interested in contrasting how variable and constant hard sphere diameters affect our simulations, so the recent VSS model is chosen for its combination of simplicity and calibrated accuracy. In fact, we find that the VSS model and constant diameter models often produce quantitatively similar results. See Section 4 for details.

The viscosity based diameter of a VSS particle is

$$\sigma = \left( \frac{5(\alpha + 1)(\alpha + 2)(m/\pi)^{1/2}(kT_{ref})^\omega}{16\alpha\Gamma(9/2 - \omega)\mu_{ref}E_t^{\omega-1/2}} \right)^{1/2} \quad (3)$$

where  $k$  is Boltzmann's constant,  $m$  is the mass of the particle,  $\omega$  is the dimensionless viscosity index and  $\alpha$  is a dimensionless constant for each gas. The constant  $\mu_{ref}$  represents the viscosity at the reference temperature ( $T_{ref} = 273K$ ) and pressure (1 atm). Finally,  $E_t = (1/2)m_r c_r^2$  is the asymptotic kinetic energy where  $m_r$  is the reduced mass

$$m_r = \frac{m_{particle_1} m_{particle_2}}{m_{particle_1} + m_{particle_2}}$$

and  $c_r$  is the relative velocity between the particles. Tabulated values for these new parameters are provided in [5, 7] and are summarized below.

Gas	$\omega$	$\mu_{ref}$ [Nsm <sup>-2</sup> ]	$\alpha$
He	0.67	$1.865 \times 10^{-5}$	1.26
Ar	0.81	$2.117 \times 10^{-5}$	1.40
Xe	0.85	$2.107 \times 10^{-5}$	1.44

Table II. VSS Molecular Parameters

## 2.7 Ionization Effects

Near the minimum radius of the bubble, collisions may become sufficiently energetic to ionize the gas atoms. Ionization exerts a very strong cooling effect on the gas, since on the order of 10eV of thermal energy is removed from the gas by each ionization event. Indeed, if such energy losses are not included, Xenon simulations can reach temperatures in excess of one million degrees Kelvin, while the inclusion of ionization cooling brings these peak temperatures down substantially (see Section 4). This clearly shows that some degree of ionization must occur during collapse, and that its cooling effects must be included for proper prediction of peak temperatures. The ions and free electrons produced by ionization will move according to coulomb forces, but the need to incorporate these effects is not as clear, and their inclusion is more difficult and expensive due to the long range effects, so

they will not be included in this first treatment. We will only consider the impact of ionization on energy accounting.

For the purpose of energy accounting, an ionization ultimately produces two losses: the energy of ionization is lost immediately, and the emitted cold electron will quickly be heated to thermal equilibrium with the gas through subsequent electron-gas collisions, thus extracting an additional one particle's worth of thermal energy by the equipartition of energy.

For our model, we will simply assume ionization occurs with probability 1 whenever the collision energy exceeds the ionization potential, we deduct a suitable amount of energy from the pair. We also we keep track of how many electrons each particle has lost, so that we can make use of the appropriate next ionization energies and calculate the local ionization levels. The direction of gas particle propagation is updated exactly as without ionization. See Section 2.3 for details.

More precisely, if the kinetic energy (in the center of mass frame) of two colliding particles is greater than the next ionization energy of either of the pair (which may already be ionized), that particle loses an additional electron. We account for the net energy loss by setting the kinetic energy of the pair to be

$$\frac{2}{3} \left( E_0 - \chi \frac{E_0}{E} \right)$$

where  $E_0$  is the original kinetic energy of the particle,  $E$  is the kinetic energy of both particles before the collision and  $\chi$  is the ionization potential of the minimally charged particle.

Note that the final kinetic energy of the pair is the initial energy, minus the ionization energy, with an additional 1/3 deducted to represent the subsequent energy lost to thermalizing the electron. This is not the only possible way to include this effect, and of course in reality this process involves losses from other gas particles besides the colliding pair, but this approach is the simplest way to include the effect.

We also do not account for subsequent electron-ion recombination to neutral atoms, although this would be interesting to include at the next level of description. In particular, this could be an interesting source of radiation as the hot spot decays.

For reference, the approximate ionization potentials used for the three noble gases are provided in Table III below.

Gas	Ion							
	Neutral	1+	2+	3+	4+	5+	6+	7+
He [34]	2.37	5.25						
Ar [34]	2.08	2.67	3.93	5.77	7.24	8.78	12.0	13.8
Xe [34, 6]	1.17	2.05	3.10	4.60	5.76	6.93	9.46	10.8

Table III. Ionization potential [MJ/mol]. Each entry represents the energy required to ionize the indicated state.

### 3 Algorithm

Efficient algorithms are needed to evolve our hard sphere model for sonoluminescence since a naive coding is prohibitively slow for anything more than a few thousand particles. To achieve this goal, we modify and extend existing methods [28] rather than develop new algorithms and codes from scratch. This section outlines the principle algorithms used to evolve our hard sphere system. Further details and basic codes are provided in [28].

#### 3.1 Cell Subdivision

The hard sphere simulation proceeds according to a time ordered sequence of collision events [28, 8]. But clearly a direct determination of the next event for a given particle is impractical in our large simulations because  $O(N)$  work is required *per particle* to examine all possible collision partners, where  $N$  is the total number of particles.

Fortunately this work can be reduced to a constant independent of  $N$  by dividing the bubble into a number of cells [28, 8]. By taking an edge length that is larger than the sphere diameter,  $\sigma$ , it is obvious that collisions can only occur between particles in the same and adjacent cells. Since we want a relatively small number of particles in each cell *and* we want the number of cells to be comparable to the number of particles in the simulation the size of the cells must be reduced as the bubble collapses. We use a straightforward subdivision procedure to accomplish this task. Initially, the bubble is subdivided into approximately  $8N$  square, identical cells. Every time the bubble declines by a factor of two in diameter, cell size is reduced by a factor of two (keeping in mind that we must stop the procedure once the cell diameters reach the particle diameter). Note that we do not need to

recompute which particle belongs to which cell after each collision. Instead, we introduce a cell crossing event and update a particle’s cell location only when the corresponding cell crossing event is processed (cf. [28, 8]).

Also note that when a collision occurs, only particles in the immediate neighborhood of the cell need to be updated. For this reason a ‘personal’ time is stored for each particle, representing the time when the particle was last updated. The entire system configuration only needs to be updated when properties (such as density, temperature etc.) are evaluated. [28, 8]

### 3.2 Event Calendar

Because we require information on when particle collisions, hard wall collisions and cell crossings occur some sort of *event calendar* is needed. This calendar will store many future events. As collisions and cell crossings occur, newly predicted collisions and cell crossings must be added to the calendar and events that are no longer relevant must be removed. [28]

Specifically, whenever particles collide their velocities are changed. This implies that future events involving these particles are no longer valid and should be removed from the calendar. It also implies that new cell crossings and collision events need to be calculated and added to the calendar. (Fortunately, the only particle collisions that need to be considered are those involving the current cell and its neighbors.) On the other hand, when a particle crosses cell boundaries previous particle collisions remain valid but the newly adjacent cells contain potential collision targets that must be examined. New cell crossing events must also be checked. As pointed out in [28], there is no way in which a collision can be missed provided all these details are taken care of correctly.

Of course, it is essential that the calendar can be managed efficiently both in terms of memory and CPU usage. To meet this requirement, we utilize the binary tree data structure described in [27, 28]. Here, each scheduled event is represented by a node in the tree. The information contained within the node identifies the time at which the event is scheduled and the event details. Calendar events are added or deleted by adding or deleting the corresponding nodes from the tree. To facilitate traversing the tree, three pointers are used to link event nodes. These point to the left and right descendents of the node and to the node’s parent. The ordering is carried out so that left hand descendents of a particular node are events scheduled to occur before the



event at the current node, while right hand descendents correspond to events that occur after it. Finally, the rapid deletion of event nodes is supported by linking event nodes into two circular lists. See [28] for details.

It is interesting that estimates of the theoretical performance of the tree structure are possible in a number of instances [18, 28]. For example, if a tree is constructed from a series of events that are randomly distributed, the average number of nodal tests to insert a new node into the tree is  $2 \log N$ . Also, the average number of cycles to delete a randomly selected node is a constant independent of  $N$ . It is noteworthy that measurements have been performed to confirm these results in actual MD simulations [27]. Our sonoluminescence simulations spend most of the CPU time on compressing the bubble from its maximum radius to the ambient radius. Since the bubble is fairly uniform in this regime, the assumption of a random distribution of events seems plausible and we expect that this type of estimate on theoretical performance should hold. (On the other hand, near the short-lived hot spot the behavior is far from equilibrium and this assumption on randomness may be invalid.) A detailed study of the theoretical performance of the tree structure will be the focus of subsequent work.

### 3.3 Average Properties

We need to evaluate spatially dependent average properties of the gas at various times. To minimize statistical fluctuations, we assume that the results are radially symmetric and average over shells that are 1/40th of the bubble radius. We calculate dimensionless values for density, temperature, velocity and average charge as follows:

- The dimensionless density is given by the density divided by the average ambient density.
- The dimensionless velocity is given by the velocity divided by the ambient speed of sound  $\sqrt{\gamma k T_0 / m}$  where  $\gamma$  is the ratio of heat capacities and  $m$  is the mass of a single particle.
- The dimensionless temperature is given by the temperature divided by the ambient temperature,  $T_0$ . Specifically,

$$T = \frac{m}{3NkT_0} \sum_i^N (v_i^2 - v_n^2)$$

where the summation is over all  $N$  particles in the shell,  $v_i$  is the speed of the  $i^{\text{th}}$  particle and  $v_n$  is the normal speed of the gas in the shell.

- Ionization is simply the average charge per particle.
- In each case we plot properties as a function of a dimensionless bubble radius,  $r$ , which equals the physical radius  $R(t)$  divided by a constant approximating the atomic diameter. For Helium this constant is chosen to be  $2.18\text{\AA}$  (see Table I). For Argon and Xenon these constants are chosen to be  $4.11\text{\AA}$  and  $5.65\text{\AA}$ , respectively. (These latter two choices represent average VSS model values at 273K and also approximate the values given in Table I).

See [28] for further details on calculating equilibrium and transport properties for hard sphere models.

## 4 Simulation Results

In this section we simulate the collapse of a sonoluminescing bubble from its maximum radius to its hot spot. Our focus is on how boundary conditions affect the interior dynamics of the collapse. Results for Helium, Argon and Xenon are presented.

The section begins with a study of the collapse of million particle bubbles and concludes by addressing how simulations vary according to ambient bubble size.

### 4.1 Helium Bubbles with Specular BCs

We first consider evolving a bubble of one million helium atoms using specular boundary conditions.

With the *constant diameter model* and *no ionization* the temperature and density increase uniformly as the bubble collapses to the minimum radius. After the minimum radius is attained, the temperature becomes hotter towards the center of the bubble and cools at the expanding outer boundary of the bubble, with a peak temperature of about 80000K reached at the center. (At these temperatures, it is clear that ionization events will occur so the remainder of our simulations consider ionization.) See Figure 2 for plots

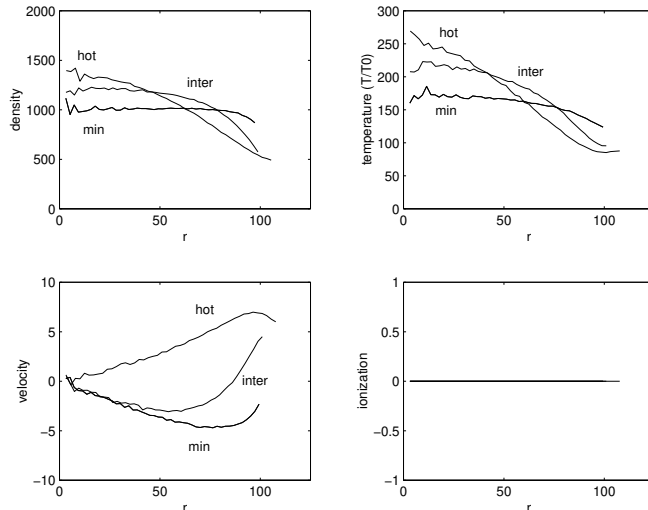


Figure 2: Helium bubble with specular BCs, constant diameter particles and no ionization. Here,  $R_{min} = 99.4$ ,  $R_{inter} = 101.0$  and  $R_{hot} = 107.7$

of the density, temperature and velocity as a function of distance from the center of the bubble at various bubble radii.

With the *constant diameter model* and *ionization* we again find that the temperature and density increase uniformly as the bubble collapses to the minimum radius. However, after the minimum radius is attained, ionization causes the temperature to cool across the entire bubble rather than just at the boundary of the bubble (although cooling occurs most rapidly at the bubble boundary). A peak temperature of about 40000K is attained at the minimum radius. It is particularly noteworthy that recorded properties are nearly constant throughout the bubble when the peak temperature occurs — See Figure 3.

Changing to the *VSS diameter model* gives very similar results, except now ionization occurs less frequently because the effective size of the particles is smaller. Because less ionization occurs, the temperature continues to increase for a short while after the minimum bubble radius leading to a peak temperature of about 45000K. See Figure 4 for details.

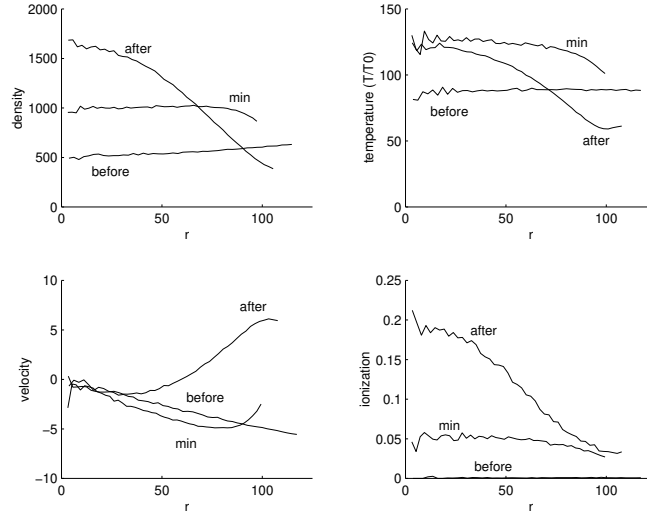


Figure 3: Helium bubble with specular BCs, constant diameter particles and ionization. Here,  $R_{before} = 117.2$ ,  $R_{min} = 99.4$  and  $R_{after} = 107.7$

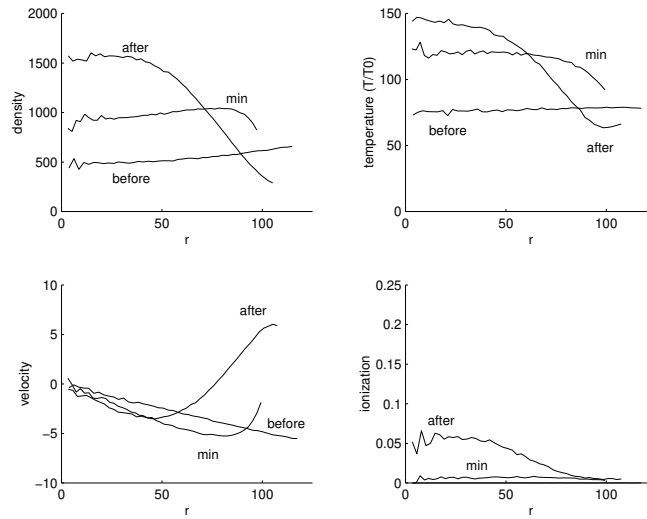


Figure 4: Helium bubble with specular BCs, VSS diameter particles and ionization. Here,  $R_{before} = 117.4$ ,  $R_{min} = 99.4$  and  $R_{after} = 107.5$

## 4.2 Helium Bubbles with Heat Bath BCs

Our next set of simulations evolve a bubble of one million helium atoms using heat bath boundary conditions and ionization.

With the *constant diameter model* the density increases dramatically at the edge of the bubble as the minimum radius is attained. Temperature and velocity are also much more profiled than for specular boundary conditions, with peaks occurring about 25 percent of the way from the boundary of the bubble to the center. No ionization has occurred at the minimum radius. For a short time after the minimum radius<sup>1</sup>, the peak temperature of the bubble continues to increase (to a maximum of 95000K), and temperature and density profiles become even more pronounced — See Figure 5. At first sight, it is counterintuitive that heat bath boundaries create conditions whereby the cooling from the boundary leads to greater energy focusing and higher peak temperatures. Perhaps cooling lowers the speed of sound and enhances the nonlinear response to the high speed  $\dot{R}$  of collapse.

Changing to the *VSS diameter model* gives very similar results, except now ionization occurs less frequently because the effective size of the particles is smaller. See Figure 6 for details.

## 4.3 Argon and Xenon Bubbles with Specular BCs

Our next set of simulations evolve million particle Argon and Xenon bubbles using specular boundary conditions and ionization.

We start by considering an Argon bubble with the *VSS diameter model*. Because the speed of sound is slower in Argon than in Helium we expect Argon simulations to exhibit much sharper profiles than Helium. This is indeed the case. Moreover, our simulation results are surprisingly similar to those for Helium with *heat bath boundaries*: Density increases at the edge of the bubble as the minimum radius is attained. Temperature and velocity are sharply profiled, with peaks occurring closer to the boundary of the bubble than to its center. Also, for a short time after the minimum radius, the peak temperature of the bubble continues to increase rapidly (to a maximum of 100000K), and temperature and density profiles become even more pronounced — See Figure 7.

---

<sup>1</sup>Note that a vacuum forms at the bubble wall after the minimum radius occurs. This is simply an artifact of using Equation 1 as the forcing equation for  $R(t)$ .

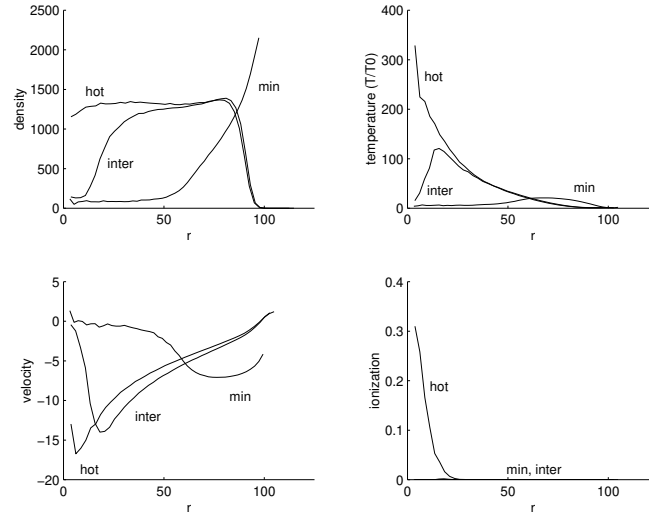


Figure 5: Helium bubble with heat bath BCs, constant diameter particles and ionization. Here,  $R_{min} = 99.4$ ,  $R_{inter} = 114.8$  and  $R_{hot} = 117.2$

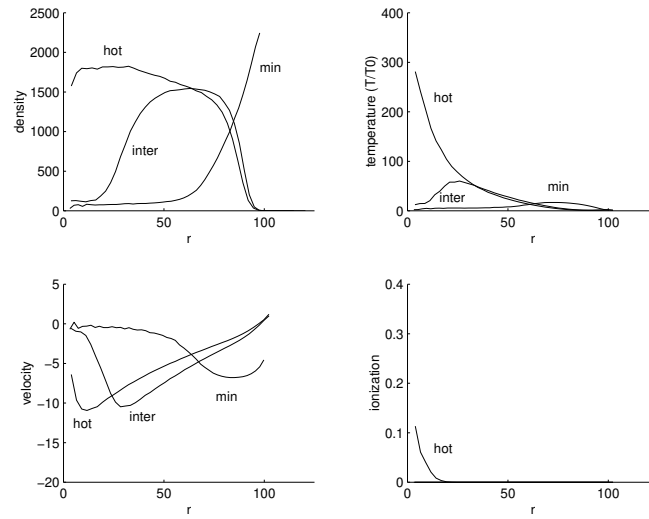


Figure 6: Helium bubble with heat bath BCs, VSS diameter particles and ionization. Here,  $R_{min} = 99.4$ ,  $R_{inter} = 117.2$  and  $R_{hot} = 123$

Constant diameter hard sphere simulations of Argon are also possible. These simulations are unique<sup>2</sup> in that the hot spot occurs before the minimum radius value of 58.2 — See Figure 8. As expected, this simulation gives sharper profiles than the corresponding model for Helium. However, since the minimum radius is close to the minimum radius allowed by the packing of the hard spheres the results are much more uniform than those derived using the VSS model for Argon. Also note that as a result of the collapse of the bubble, energy stored at the maximum radius is converted into heating, ionization and kinetic energy of the local center of mass. From Figure 8 one can estimate these quantities. The average temperature of the atoms is 30000K which is a thermal energy of about 3.75 eV/atom. As half the atoms are ionized, the ionization energy is about 8 eV/atom. Since electrons have about the same thermal energy as the ions, their energy is about 2 eV/atom. Taken together, these channels add to about 21 eV/atom which is less than the 25 eV/atom available in the initial state but the difference is within the accuracy of the energy estimates. For Helium at the hot spot, the energy of the hard sphere (plus ionization) is substantially less than the energy stored at  $R_m$ . This can be attributed to the fact that  $a_{hs}/a \approx 0.60$ . For Argon, almost all the stored energy ends up in the hard sphere gas since  $a_{hs}$  is much closer to  $a$ ;  $a_{hs}/a \approx 0.91$ . In both cases, inclusion of a self-consistent boundary condition at the wall will account for any further energy discrepancies. Of course, in a physical system, energy will diminish due to acoustic radiation and thermal losses through the boundary of the bubble and we expect this to constitute a strong effect.

Simulations for Xenon bubbles with the *VSS diameter model* were also carried out. Because the speed of sound is slower in Xenon than in Argon we expect Xenon simulations to exhibit even sharper profiles than Argon. Indeed, this is the case and temperatures of up to 300000K were obtained despite the occurrence of multiple ionization (exceeding 4 per particle at the center) — See Figure 9.

A proviso for the Xenon data is that these calculations bog down before the minimum radius is attained when the constant diameter model is used, whereas the Helium data is hardly affected by this modification. The explanation lies in the consistency of the minimum bubble radius ( $\sim a$ ) and

---

<sup>2</sup>This behavior may be related to the consistency of the minimum bubble radius and the hard sphere radius. See the case of Xenon below.

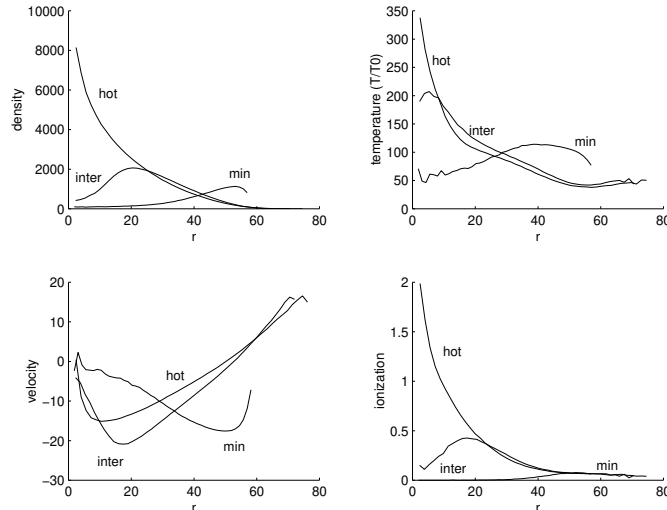


Figure 7: Argon bubble with specular BCs, VSS diameter particles and ionization. Here,  $R_{min} = 58.2$ ,  $R_{inter} = 72.0$  and  $R_{hot} = 76.2$

the hard sphere radius for Xenon. Specifically, the minimum radius of the bubble wall is less than the minimum radius allowed by the packing of hard spheres. On the other hand, Xenon simulations carried out using the VSS model are relatively insensitive to changes in  $a$ . For example, increasing  $a$  by 30% changes the peak temperature by about 35%, and leaves the qualitative features invariant. Note that in this case,  $a_{hs} < a$  as with Helium simulations.

#### 4.4 Argon and Xenon Bubbles with Heat Bath BCs

We now consider the evolution of million particle Argon and Xenon bubbles using Heat Bath boundary conditions and ionization.

Applying the *VSS diameter model* to an Argon bubble gives results that have the same qualitative features as the corresponding Helium simulation, except that all properties are much more sharply profiled. Indeed, temperatures of up to 300000K were obtained in this simulation showing (once again) that heat bath boundaries create conditions whereby the cooling from the boundary leads to greater energy focusing and higher peak temperatures than specular boundary conditions. See Figure 10 for details.



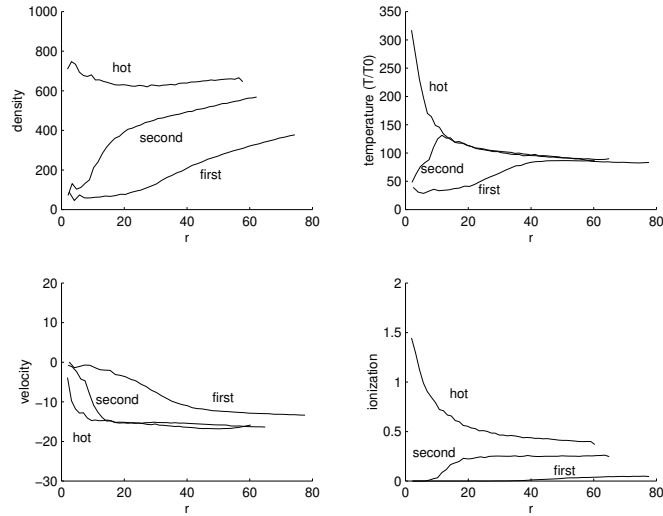


Figure 8: Argon bubble with specular BCs, constant diameter particles and ionization. Here,  $R_{first} = 77.6$ ,  $R_{second} = 64.9$  and  $R_{hot} = 60.3$

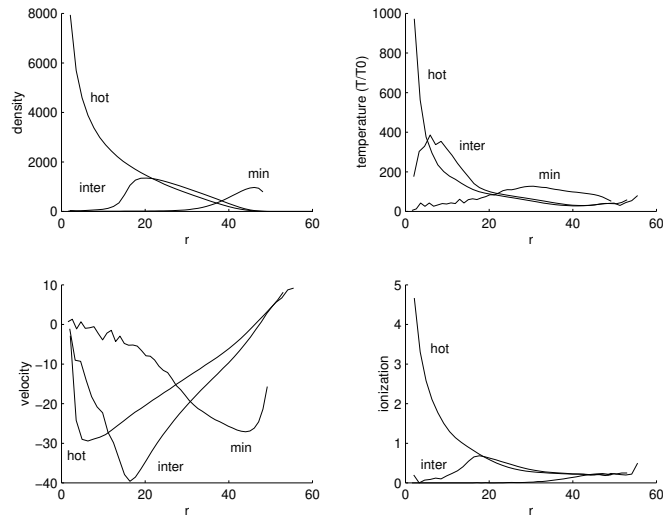


Figure 9: Xenon bubble with specular BCs, VSS diameter particles and ionization. Here,  $R_{min} = 49.2$ ,  $R_{inter} = 62.2$  and  $R_{hot} = 66.7$

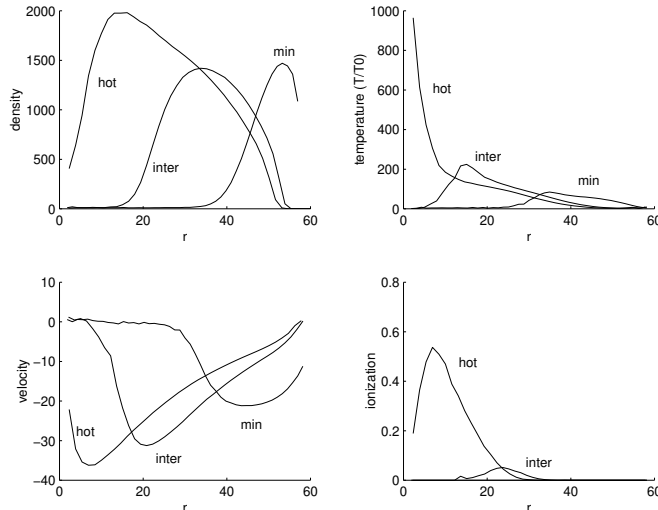


Figure 10: Argon bubble with heat bath BCs, VSS diameter particles and ionization. Here,  $R_{min} = 58.2$ ,  $R_{inter} = 68.1$  and  $R_{hot} = 73.2$

Simulations for Xenon bubbles with the *VSS diameter model* were also carried out. Because the speed of sound is slower in Xenon than in Argon, Xenon simulations exhibit even sharper profiles than Argon. Indeed, temperatures of up to 500000K were obtained. See Figure 11 for details.

As discussed in the previous section, the constant diameter model for Xenon is not able to compute down to the minimum radius since that radius is smaller than the minimum packing radius of the hard sphere gas. On the other hand, Argon calculations are possible. These simulations are qualitatively similar to the constant diameter model for Helium, but produce a more highly ionized gas (reaching an average charge of +6 per particle near the center) and much higher temperatures (up to 1.5 million K) than any other simulations that were considered. Because such extreme values arise it seems likely the constant diameter model for Argon also experiences a significant consistency problem near the minimum radius.

## 4.5 Flashwidths

An important experimental measurement for SL bubbles is the flash width, i.e. the duration of the light emission, because this constrains the possible

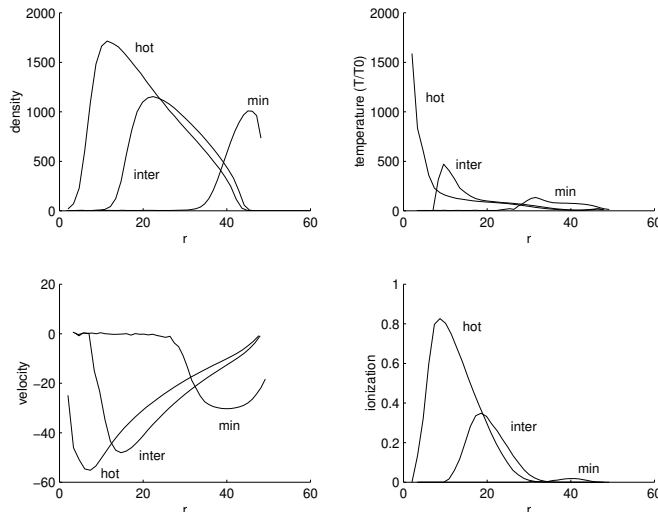


Figure 11: Xenon bubble with heat bath BCs, VSS diameter particles and ionization. Here,  $R_{min} = 49.2$ ,  $R_{inter} = 60.8$  and  $R_{hot} = 63.7$

light emission mechanisms and thus provides a point of validation for any proposed model or theory. Since our simulations do not include the fundamental atomic excitation or charge acceleration effects responsible for radiation, the current model does not directly yield a flashwidth.

However, an estimated flash width can be obtained from the computed temperature as a function of time. If we assume that whatever process is responsible for the light emission is strongly dependent on the current temperature, and that it does not appreciably alter the gross gas dynamics, the flashwidth at a particular color is simply the length of time which the temperature exceeds the appropriate turn-on threshold. In this case, the peak temperature as a function of time is our key diagnostic quantity.

Our simulations (Figure 12) show that emission from an adiabatic compression lacks a strong, sharp temperate spike in time, and thus the associated flash from this model would be longer and would be comprised of lower energy photons. In contrast, the heat bath boundary conditions yield sharp transient spike in temperature, and thus this model predicts a much shorter flash which is comprised of higher energy photons. In both cases it appears that the width of the spike roughly doubles as the number of particles in the bubble increases by factors of 10, from  $N = 10^4$  to  $N = 10^6$ . Since each

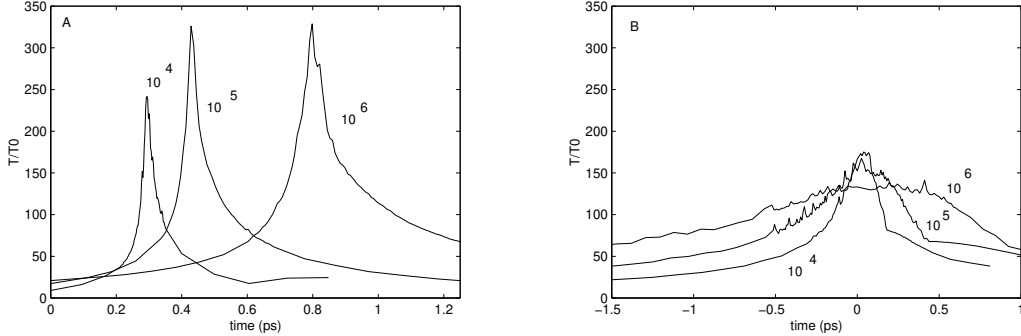


Figure 12: Helium peak bubble temperature vs. time with  $time = 0$  marking the time corresponding to the minimum radius. (A) Heat Bath boundary conditions. (B) Specular Boundary conditions.

factor of 8 in particle number corresponds to a doubling of the ambient bubble radius  $R_0$ , this amounts to essentially a predicted linear scaling between flash width and ambient bubble radius.

In both plots, the curves for  $N = 10^5$  and  $N = 10^4$  particles were derived by averaging over 10 and 20 simulations respectively in order to keep statistical fluctuations to an acceptable level. The  $N = 10^6$  simulation required just a single simulation for robust statistics.

## 5 Summary and Future Work

Sonoluminescence is well suited to investigation by Molecular Dynamics because the range of densities and time scales is large, yet the number of particles involved is relatively small. Because the phenomena still poses experimentally difficult, unsolved questions regarding its mechanism and ultimate energy focusing energy potential, we feel it is an excellent subject for much more detailed MD investigations than the initial effort we have presented here.

In this paper, we introduced a simple model for the interior dynamics of single noble gas bubble sonoluminescence, as a hard sphere gas driven by a spherical piston controlled by the Rayleigh-Plesset equation. Energy losses due to ionization were also accounted for. We considered both constant and

variable radius hard sphere models, and these lead to quantitatively similar results. Fast, tree-based algorithms allowed us to evolve million particle systems through the entire collapse process. Our calculations indicate that extreme energy focusing occurs within the bubble which in some cases is driven by a shock-like compression in the gas. Peak temperatures range from 40,000 K for He to 500,000 K for Xe. These are accompanied by high levels of ionization during the final collapse, and formation of a transient, high density plasma state seems quite likely.

The imposition of a thermal boundary condition at the wall of the bubble leads to greatly increased energy focusing and non-uniformity within a collapsing bubble. In any case, the predicted flash width scales roughly linearly with the ambient bubble radius.

There are a variety of interesting directions for future research in this problem. For example, our simulations simply treat the bubble wall as a piston moving in with a prescribed velocity. A natural improvement would be to couple the internal molecular dynamics to the wall velocity to obtain a self-consistent bubble motion and internal dynamics. This could be done by coupling to Euler or Navier Stokes models for the surrounding fluid. This may be particularly important for accurately computing the dynamics through the point of minimum radius. In our present model there may be over compression of the gas in some simulations as the minimum radius is approached, since the prescribed piston motion does not respond to the rapid increase in the internal gas pressure. Conversely, when the piston retracts after this point, a nonphysical gap often develops between the bubble boundary and the outer extent of the gas, which may under-compress the gas.

Another important area for future research is adding in water vapor into the bubble interior. This provides a potentially important cooling mechanism, which may strongly modulate the light emission and energy focusing, and may explain the strong ambient temperature dependence of the emitted light intensity. We have done preliminary investigations of this, and these show that water evaporation from the bubble surface into the interior must be included to avoid rapid expulsion of the water vapor. It is also possible that the water could be directly involved in the light emission, when it is properly included in the model.

Other bubble collapse geometries could also be considered, and these may have different energy focusing characteristics. For example, one could

consider a nonspherical collapse, hemi-spherical bubbles collapsing on a solid surface, or consider collapse geometries appropriate for bubble jetting scenarios. Similarly, one could see if special collapse profiles can be used to reach much higher internal temperatures, and otherwise explore the extremes of the energy focusing potential. Perhaps a mode could even be found in which small amounts of deuterium-deuterium fusion could be induced, assuming there is deuterium gas in the bubble as well.

Including additional atomic physics such as atomic excitation, rotational and vibrational degrees of freedom (needed for non-noble gases or water vapor) and electron-ion recombination would all allow for more accurate energy accounting, and may also be directly related to light emission mechanisms.

Another major direction would be to include electric field effects into the the simulation. Algorithms for such models must treat long range electrostatic interactions to avoid incurring serious errors. They must also be able to evaluate long range forces efficiently since calculating interactions pairwise becomes expensive for more than a few thousand particles. For these reasons, multipole methods are particularly attractive— they use a hierarchy of spatial subdivisions and a multipole expansion to evaluate interactions with little more than linear effort in the number of particles. See [13, 12] for details and see also [28] for further references on methods for evaluating long range forces. This would potentially allow direct simulation of the ions and electrons produced as well, which, along with including atomic excitation, would allow direct simulation of the light emitting processes. With these effects included, an extremely detailed picture of the SL phenomena could be laid out.

Of course, larger scale, parallel simulations are essential to actually achieve direct comparisons with present SL experiments. Because the simple hard sphere interactions are quite local, the system should be amenable to parallelization. We expect that the cost (in collision count) for a hard sphere MD simulation scales roughly like  $N^{4/3}$ , where  $N$  is the number of particles, since the collapse time from the ambient to the minimum radius scales linearly with  $R_0$  (and so we conjecture that the collision rate also increases roughly linearly with the  $R_0$ ). Thus simulations using one hundred times as many particles (i.e.  $N = 10^8$ ) would require 500 times as much computer time assuming near optimality in the algorithm. This is somewhat beyond the range of a single supercomputer CPU, but would become quite practical on a 100 node system of workstation-grade CPUs.

Finally, it would be of great interest to investigate where less costly continuum models and Monte Carlo simulations are appropriate for studying sonoluminescence and to develop techniques for coupling these methods to detailed molecular dynamics simulations near the light emitting hot spot, in order to produce more complete models with greater predictive validity.

There is also a great deal to explore experimentally. One example relevant to our study is that it would be useful to measure flashwidth as a function of ambient bubble radius (or, in practice, intensity and frequency of the driving sound field), for comparison with the scaling predictions of MD and other models.

## 6 Acknowledgments

We thank D.B. Hash, A.L. Garcia and P.H. Roberts for valuable discussions.

## References

- [1] B.P. Barber, R.A. Hiller, R. Lofstedt, S.J. Putterman, and K.R. Weninger. Defining the unknowns of sonoluminescence. *Phys. Reports*, 281(2):66–143, 1997.
- [2] B.P. Barber and S.J. Putterman. Observation of synchronous picosecond sonoluminescence. *Nature*, 352:318–320, 1991.
- [3] B.P. Barber, C.C. Wu, R. Lofstedt, P.H. Roberts, and S.J. Putterman. Sensitivity of sonoluminescence to experimental parameters. *Phys. Rev. Lett.*, 72:1380, 1994.
- [4] G.A. Bird. Monte Carlo simulation in an engineering context. *Progr. Astro. Aero.*, 74:239–255, 1981.
- [5] G.A. Bird. *Molecular Gas Dynamics and the Direct Simulation of Gas Flows*. Oxford University Press, 1998.
- [6] T.A. Carlson, Jr. C.W. Nestor, and N. Wasserman. Calculated ionization potentials for multiply charged ions. *Atomic Data*, 2:63–99, 1970.

- [7] S. Chapman and T.G. Cowling. *The mathematical theory of non-uniform gases*. Cambridge University Press, third edition, 1970.
- [8] J.J. Erpenbeck and W.W. Wood. Molecular dynamics techniques for hard-core systems. In B.J. Berne, editor, *Modern Theoretical Chemistry*, volume 6B, pages 1–40. Plenum, New York, 1977.
- [9] S.J. Putterman et al. Is there a simple theory of sonoluminescence. *Nature*, To Appear.
- [10] H. Frenzel and H. Schultes. Lumineszenz im ultraschallbeschickten wasser. *Z. phys. Chem.*, B27:421–424, 1934.
- [11] D.F. Gaitan and L.A. Crum. Sonoluminescence and bubble dynamics for a single, stable, cavitation bubble. *J. Acoust. Soc. Am.*, 91(6):3166–3183, 1992.
- [12] L. Greengard. *The Rapid Evaluation of Potential Fields in Particle Systems*. MIT Press, Cambridge, 1988.
- [13] L. Greengard and V. Rokhlin. A fast algorithm for particle simulations. *J. Comp. Phys.*, 73:325, 1987.
- [14] H.P. Greenspan and A. Nadim. On sonoluminescence of an oscillating gas bubble. *Phys. Fluids A*, 5:1065–1067, 1993.
- [15] H.A. Hassan and D.B. Hash. A generalized hard-sphere model for Monte Carlo simulations. *Phys. Fluids A*, 5:738–744, 1993.
- [16] S. Hilgenfeldt, S. Grossmann, and D. Lohse. A simple explanation of light emission in sonoluminescence. *Nature*, 398(6726):402–405, 1999.
- [17] J.H. Jeans. *Introduction to the Kinetic Theory of Gases*. Cambridge University Press, 1940.
- [18] D.E. Knuth. *Sorting and Searching*, volume 3 of *The Art of Computer Programming*. Addison-Wesley, 1973.
- [19] L. Kondic, J.I. Gersten, and C. Yuan. Theoretical studies of sonoluminescence radiation - radiative transfer and parametric dependence. *Phys. Rev. E*, 52(5):4976–4990, 1995.



- [20] K. Koura and H. Matsumoto. Variable soft sphere molecular model for inverse-power-law or Lennard-Jones potential. *Phys. Fluids A*, 3:2459–2465, 1991.
- [21] K. Koura and H. Matsumoto. Variable soft sphere molecular model for air species. *Phys. Fluids A*, 4:1083–1085, 1992.
- [22] W.C. Moss, D.B. Clarke, and D.A. Young. Calculated pulse widths and spectra of a single sonoluminescing bubble. *Science*, 276:1398–1401, 1997.
- [23] W.C. Moss, D.A. Young, J.A. Harte, J.L. Levatin, B.F. Rozsnyai, G.B. Zimmerman, and I.H. Zimmerman. Computed optical emissions from a sonoluminescing bubble. *Phys. Rev. E*, 59(3):2986–2992, 1999.
- [24] S.J. Putterman and K.R. Weninger. Sonoluminescence: How bubbles turn sound into light. *Ann. Rev. Fluid Mech.*, 32:445, 2000.
- [25] A.O. Rankine. On the variation with temperature of the viscosities of the gases of the Argon group. *Proc. Roy. Soc. A*, 84:181–192, 1910.
- [26] A.O. Rankine. On the viscosities of the gases of the Argon group. *Proc. Roy. Soc. A*, 83:516–525, 1910.
- [27] D.C. Rapaport. The event scheduling problem in molecular dynamics simulation. *J. Comput. Phys.*, 34:184–201, 1980.
- [28] D.C. Rapaport. *The Art of Molecular Dynamics Simulation*. Cambridge University Press, 1998.
- [29] W.B. Russel, D.A. Saville, and W.R. Schowalter. *Colloidal Dispersions*. Cambridge University Press, New York, 1989.
- [30] P.R. Temple. Sonoluminescence from the gas of a single bubble. Master’s thesis, University of Vermont, 1970.
- [31] V.Q. Vuong, A.J. Szeri, and D.A. Young. Shock formation within sonoluminescence bubbles. *Phys. Fluids*, 11(1):10–17, 1999.
- [32] K.R. Weninger, C. Camara, and S.J. Putterman. *Physical Review E*, 2001.

- [33] K.R. Weninger, P.G. Evans, and S.J. Putterman. Time correlated single photon mie scattering from a sonoluminescing bubble. *Phys. Rev. E*, 61(2):1020–1023, 2000.
- [34] R.C. West, editor. *Handbook of Chemistry and Physics*. CRC Press, Boca Raton, 1985.
- [35] C.C. Wu and P.H. Roberts. Shock-wave propagation in a sonoluminescing gas bubble. *Phys. Rev. Letters*, 70(22):3424–3427, 1993.
- [36] K. Yasui. Alternative model of single-bubble sonoluminescence. *Phys. Rev. E.*, 56(6):6750–6760, 1997.